Eur. J. Mineral., 36, 605–614, 2024
https://doi.org/10.5194/ejm-36-605-2024

European Journal of Mineralogy
Open Access

Rotherkopfite, $KNa_2(Fe^{2+}_{2.5}Ti^{4+}_{1.5})Fe^{2+}(Si_4O_{12})_2$, a new neptunite-group mineral without essential lithium, from Rother Kopf, Eifel volcanic fields, Germany

Anthony R. Kampf[1], Gerhard Möhn[2], Chi Ma[3], George R. Rossman[3], Joy Désor[2], and Yunbin Guan[3]

[1]Mineral Sciences Department, Natural History Museum of Los Angeles County, 900 Exposition Boulevard, Los Angeles, CA 90007, USA
[2]independent researcher
[3]Division of Geological and Planetary Sciences, California Institute of Technology, Pasadena, CA 91125, USA

Correspondence: Anthony R. Kampf (akampf@nhm.org)

Received: 16 May 2024 – Revised: 15 June 2024 – Accepted: 22 June 2024 – Published: 19 August 2024

Abstract. Rotherkopfite, $KNa_2(Fe^{2+}_{2.5}Ti^{4+}_{1.5})Fe^{2+}(Si_4O_{12})_2$, is a new member of the neptunite group, from Rother Kopf, Roth, near Gerolstein, Eifel volcanic fields, Rhineland-Palatinate, Germany. It is found in cavities in a quartz–sanidine xenolith embedded in a vesicular alkaline basalt and is associated with fluorophlogopite and an amphibole supergroup mineral that is zoned from potassic-magnesio-fluoro-arfvedsonite on the exterior to potassic-fluoro-richterite in the core. It is presumed to have formed as the result of contact metasomatism of the xenolith by the alkaline basalt melt. Rotherkopfite occurs as brownish-red equant or tabular crystals, up to about 0.2 mm in maximum dimension. The mineral has a light-orange streak, a vitreous lustre, a Mohs hardness of ~ 4.5, a brittle tenacity, a curved fracture and a density of 3.20(2) g cm^{-3}. Optically, rotherkopfite crystals are biaxial (+), with $\alpha = 1.668(5)$, $\beta = 1.678(5)$, $\gamma = 1.720(5)$ (white light) and $2V(\text{meas}) = 53.2(6)°$. The empirical formula from electron microprobe analyses, secondary ion mass spectrometry and structure refinement is $(K_{0.87}Na_{0.20})_{\Sigma 1.07}(Na_{1.99}Ca_{0.01})^{M1+M2}_{\Sigma 2.00}(Fe^{2+}_{1.66}Ti_{1.48}Mg_{0.79}Mn_{0.02})^{M3}_{\Sigma 3.95}(Fe^{2+}_{0.64}Li_{0.16}Ti_{0.15}Al_{0.01})_{\Sigma 0.96}(Si_{8.00}O_{24})$. Rotherkopfite is monoclinic with space group $C2/c$ and unit-cell parameters $a = 16.4599(17)$, $b = 12.5457(6)$, $c = 10.0487(7)$ Å, $\beta = 115.669(7)°$, $V = 1870.3(3)$ Å^3 and $Z = 4$. The crystal structure ($R_1 = 0.0268$ for 1324 reflections with $I > 2\sigma_I$) is based on two interwoven three-dimensional frameworks: (1) a silicate framework made up of pyroxene-like chains of corner-sharing SiO_4 tetrahedra and (2) an octahedral framework made up of chains of edge-sharing metal–oxygen octahedra. The two interwoven frameworks are bound to one another by corner sharing. K and Na are hosted in channels in the combined framework.

1 Introduction

Although the neptunite group has not been formally accepted by the International Mineralogical Association (IMA), it is generally considered to include neptunite, magnesioneptunite, manganoneptunite and watatsumiite. The new mineral rotherkopfite can now be added to that list. The general formula can be given as $KNa_2(M1_2M2_2)M3(Si_4O_{12})_2$, where the similar octahedrally coordinated $M1$ and $M2$ sites are grouped for nomenclature purposes and may contain Fe^{2+}, Mn^{2+}, Mg^{2+}, Ti^{4+} and V^{4+}. Until now, the $M3$ site has been dominated by Li^+; rotherkopfite is the first mineral with the neptunite structure in which the $M3$ site is dominated by Fe^{2+} rather than Li^+. The five minerals with the neptunite structure are listed with their formulas in Table 1.

The name rotherkopfite is based on the name of the type locality. The mineral and its name have been approved by the IMA Commission on New Minerals, Nomenclature and Classification (CNMNC), proposal IMA2023-032a (Warr symbol: Rkp). The holotype (consisting of seven small rock

Table 1. Minerals with the neptunite structure (neptunite-group minerals).

Name	Ideal formula	$M1+M2$	$M3$
Neptunite[a]	$KNa_2LiFe^{2+}_2Ti_2(Si_4O_{12})_2$	$Fe^{2+}_2Ti^{4+}_2$	Li
Magnesioneptunite[b]	$KNa_2LiMg_2Ti_2(Si_4O_{12})_2$	$Mg_2Ti^{4+}_2$	Li
Manganoneptunite[c]	$KNa_2LiMn^{2+}_2Ti_2(Si_4O_{12})_2$	$Mn^{2+}_2Ti^{4+}_2$	Li
Watatsumiite[d]	$KNa_2LiMn^{2+}_2V_2(Si_4O_{12})_2$	$Mn^{2+}_2V^{4+}_2$	Li
Rotherkopfite	$KNa_2Fe^{2+}(Fe^{2+}_{2.5}Ti^{4+}_{1.5})(Si_4O_{12})_2$	$Fe^{2+}_{2.5}Ti^{4+}_{1.5}$	Fe^{2+}

[a] Kunz et al. (1991). [b] Karimova et al. (2012). [c] Zolotarev et al. (2007). [d] Matsubara et al. (2003).

fragments) is deposited in the collections of the Natural History Museum of Los Angeles County, 900 Exposition Boulevard, Los Angeles, CA 90007, USA, catalogue number 76283.

2 Occurrence and associated minerals

Rotherkopfite was found at Rother Kopf, Roth, near Gerolstein, Eifel volcanic fields, Rhineland-Palatinate, Germany (50°14′47″ N, 06°37′23″ E). Rother Kopf is also the type locality for emmerichite (Chukanov et al., 2014) and günterblassite (Chukanov et al., 2012). The new mineral occurs in cavities in a xenolith embedded in a vesicular alkaline basalt. The xenolith is composed mostly of quartz and sanidine. Other minerals found in the cavities are fluorophlogopite and an amphibole supergroup mineral that is zoned from potassic-magnesio-fluoro-arfvedsonite on the exterior to potassic-fluoro-richterite in the core. Rotherkopfite is presumed to have formed as the result of contact metasomatism of the xenolith by the alkaline basalt melt.

3 Physical and optical properties

Rotherkopfite occurs as equant to tabular crystals up to about 0.2 mm in maximum dimension (Fig. 1). The complex and variable morphology and small crystal size made measurement of forms very difficult. Some tabular crystals are flattened on $\{10\bar{1}\}$, and others are flattened on {010}. One measured crystal consists of the forms {100}, {001}, {110} and $\{10\bar{1}\}$. Careful visual examination of the lower crystal in Fig. 1 indicates it to be consistent with the crystal drawing shown in Fig. 2, which consists of the forms {010}, {001}, $\{10\bar{1}\}$, $\{11\bar{1}\}$, {201}, {221} and $\{30\bar{1}\}$. No twinning was observed.

The colour is dark brownish red, and the streak is light orange. The mineral has a vitreous lustre and is transparent. No fluorescence was observed in either long- or short-wave ultraviolet illumination. The Mohs hardness is about 4.5 based on scratch tests. No cleavage was observed. The tenacity is brittle, and the fracture is curved. The density measured by flotation in mixtures of methylene iodide and toluene is 3.20(2) g cm^{-3}. The density calculated from the empirical formula and single-crystal cell is 3.271 g cm^{-3}. The same calculated value was obtained for the empirical formula and single-crystal unit-cell parameters. At room temperature, rotherkopfite is insoluble in concentrated HCl.

Optically, rotherkopfite crystals are biaxial (+), with $\alpha = 1.668(5)$, $\beta = 1.678(5)$ and $\gamma = 1.720(5)$ (determined in white light). The $2V$ measured using extinction data analysed with EXCALIBRW (Gunter et al., 2004) is 53.2(6)°, and the calculated $2V$ is 53.1°. The interference figure could not be viewed, so the dispersion could not be determined. The optical orientation was also not determined. No pleochroism was observed. The Gladstone–Dale compatibility index (Mandarino, 1981) is 0.031 (excellent) based on the empirical formula and the single-crystal cell.

4 Chemical composition

Crystals of rotherkopfite were analysed at Caltech on a JEOL JXA-iHP200F field-emission electron microprobe (EPMA) in WDS mode (10 points on 2 crystals) and on a CAMECA IMS 7f-GEO secondary ion mass spectrometer (SIMS) (3 points on 1 crystal for Li). EPMA analytical conditions were 15 kV accelerating voltage, 20 nA beam current and 5 µm beam diameter. The primary ion beam used in SIMS analysis was a focused −12.5 kV $^{16}O^-$ beam of 0.3 nA and ∼ 5 µm in diameter. Analytical data are given in Table 2.

The empirical formula (based on 24 O apfu), with major elements allotted to structural sites in accord with OccQP (see below) and with the similar $M1$ and $M2$ sites grouped, is $(K_{0.87}Na_{0.20})_{\Sigma 1.07}(Na_{1.99}Ca_{0.01})_{\Sigma 2.00}$ $^{M1+M2}(Fe^{2+}_{1.66}Ti_{1.48}Mg_{0.79}Mn_{0.02})_{\Sigma 3.95}$ $^{M3}(Fe^{2+}_{0.64}Li_{0.16}Ti_{0.15}Al_{0.01})_{\Sigma 0.96}(Si_{8.00}O_{24})$. Note that for classification purposes the $M3$ site should be considered separately from the $M1$ and $M2$ sites. This is based on the significantly longer average M–O bond length for the $M3$ site and the strong preference of Li for this site as evidenced both by our analysis of site occupancies in rotherkopfite using OccQP and by the dominance of Li in this site in other miner-

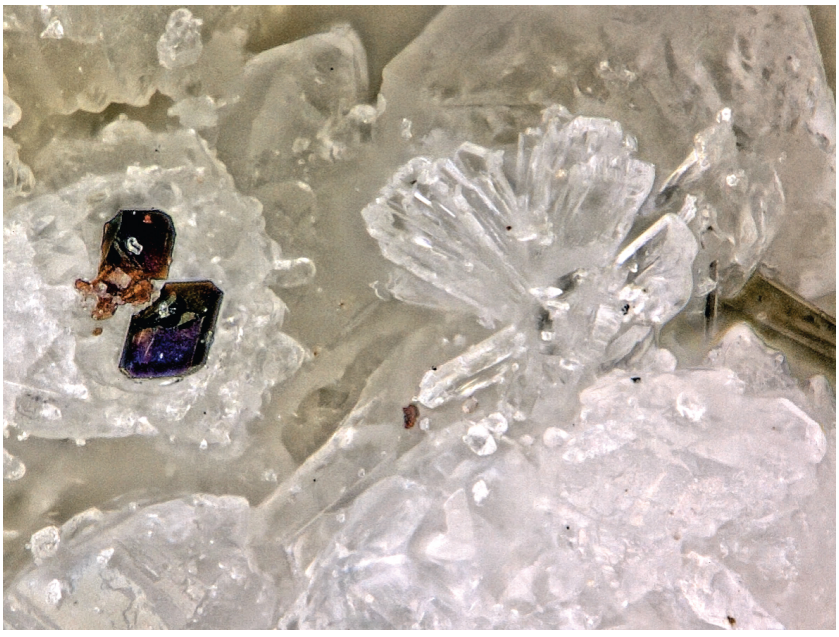

Figure 1. Brownish-red rotherkopfite crystals with spray of sanidine crystals on quartz on holotype specimen 76283; the field of view is 0.5 mm across.

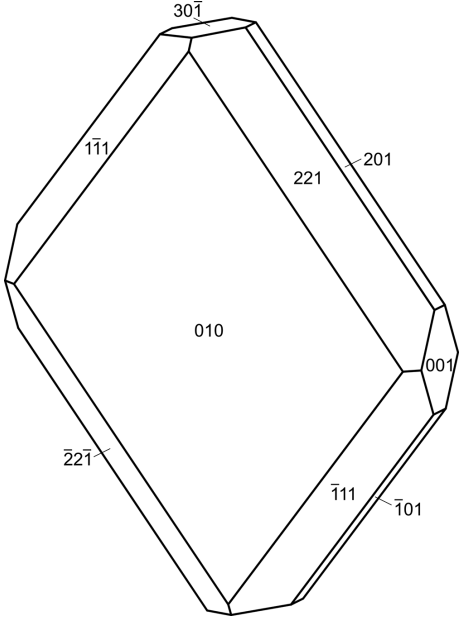

Figure 2. Crystal drawing of the rotherkopfite crystal in Fig. 1; clinographic projection is in nonstandard orientation, **a** vertical.

Table 2. Analytical data (wt %) for rotherkopfite.

Constituent	Mean	Range	SD	Standard
K_2O	4.40	4.31–4.44	0.04	microcline
Na_2O	7.30	7.10–7.59	0.16	albite
Li_2O	0.25	0.24–0.25	0.01	NBS610
MgO	3.44	2.85–4.36	0.61	forsterite
CaO	0.04	0.03–0.07	0.01	anorthite
FeO	17.84	17.50–18.65	0.33	fayalite
MnO	0.12	0.10–0.14	0.02	Mn_2SiO_4
Al_2O_3	0.05	0.02–0.08	0.02	anorthite
TiO_2	14.01	12.20–15.09	1.03	TiO_2
SiO_2	51.82	50.99–52.33	0.41	anorthite
Total	99.27			

* Based on the structure (O = 24 apfu).

als with the neptunite structure (see below). The simplified formula is $(K,Na)Na_2(Fe^{2+},Ti,Mg)_4(Fe^{2+},Li,Ti)(Si_4O_{12})_2$, and the ideal formula is $KNa_2(Fe^{2+}_{2.5}Ti^{4+}_{1.5})Fe^{2+}(Si_4O_{12})_2$, which requires K_2O 4.90, Na_2O 6.45, FeO 26.17, TiO_2 12.47 and SiO_2 50.01, for a total of 100 wt %. This end-member formula is derived from the charge constraint +13 to which $M1+M2+M3$ sites are subject. As a result, the dominant endmember charge arrangement is $^{M1}(2^+_2)^{M2}(2^+_{2.5}4^+_{1.5})^{M3}(2^+) = +13$.

5 Raman and infrared spectroscopy

Raman spectroscopy was attempted on a Horiba XploRA PLUS using both 532 and 785 nm diode lasers; however, rotherkopfite is too sensitive to both the 532 and 785 nm lasers, even at low power to record a usable spectrum.

Fourier transform infrared (FTIR) spectroscopy was done using a Thermo Nicolet iS50 FTIR and a Nicolet Continuum FTIR microscope with a 15× all-reflective lens and a

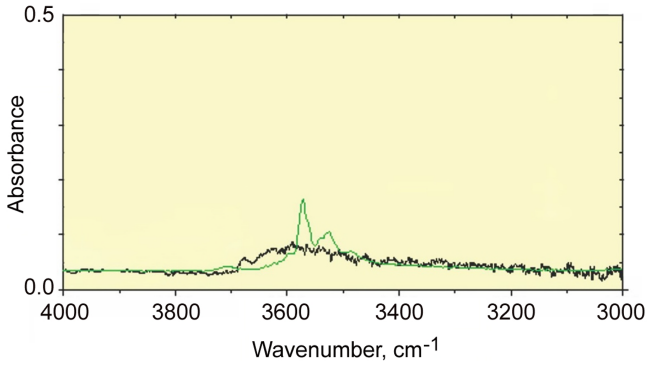

Figure 3. The FTIR spectrum of rotherkopfite (black) in the OH stretching region compared with that of nominally anhydrous olivine (green).

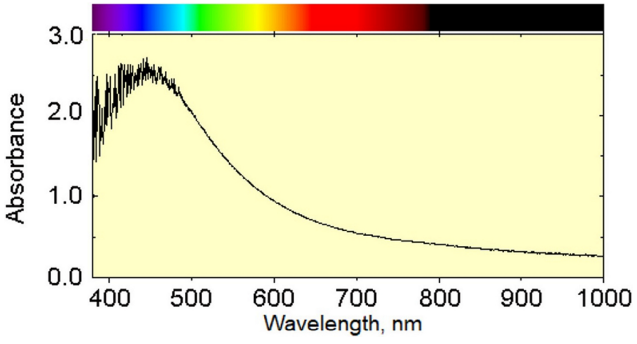

Figure 4. The optical absorption spectrum of rotherkopfite in the polarization direction in which the absorption centred at about 450 nm was apparent.

MCT-A (Hg–Cd telluride) detector with a calcium fluoride beam splitter. The spectrum, focusing in particular on the OH-stretching region (4000–3000 cm^{-1}), was acquired with 2000 scans at four-wavenumber resolution using unpolarized light. The area in the sample that was measured was masked with a 25 × 40 µm rectangular aperture that fit entirely within the area of the rotherkopfite crystal. The small size and irregular thickness of the crystal (maximum thickness 66 µm) were less than ideal.

In Fig. 3, the FTIR spectrum of rotherkopfite from 4000–3000 cm^{-1} is compared to that of a nominally anhydrous olivine (KLV-23) from the Kaalvallei kimberlite, South Africa (Bell et al., 2003). Both spectra were normalized to 100 µm thickness. The olivine is known to contain 140(20) H_2O ppm by weight bound in the olivine as OH groups. The weakness of the rotherkopfite spectrum indicates that neither water nor OH is a major stoichiometric constituent of the phase. The relative width of the rotherkopfite spectrum in the 3400–3700 cm^{-1} region and lack of significant sharper features, such as those that appear in the olivine spectrum, suggest that the minor hydrous component in the rotherkopfite consists mostly of absorbed water rather than bound OH^- ions or H_2O molecules. Such types of low-intensity water features are frequently seen in the spectra of anhydrous minerals.

6 Optical absorption spectroscopy

Optical absorption spectra were obtained in the 380–1100 nm region using a microspectrometer system described by Rossman and Taran (2001). A portion of a 151 µm long crystal of rotherkopfite approximately 39 µm wide was used as the sample with the least dark colour. The sample contained a significant number of inclusions that diminished the optical throughput of the sample.

The sample used for the optical absorption spectrum was the carbon-coated sample mounted for the electron microprobe analysis. A background spectrum that was run through the glass and the thin carbon coat was used to compensate for the absorption by the carbon coat. The sample in the mount was measured as 38.4 µm thick, most likely meaning that the actual sample was a bit thinner than that due to a thin epoxy layer holding the crystal to the glass slide.

The spectrum was run in two polarizations corresponding to having the $\boldsymbol{E}$ vector aligned with the long and short directions of the crystal. Only when the spectrum was obtained polarized along the long direction of the crystal did an absorption band centred at about 449 nm appear (Fig. 4). Its full width at half height was determined to be about 7390 cm^{-1}. Given the thinness of the crystal, the 449 nm band must be considered intrinsically intense.

Intervalence charge transfer (IVCT) bands can be much more intense than the isolated single ion absorptions, leading to the conclusion that the intense colour of the rotherkopfite crystal is due to an IVCT interaction. In several minerals, Fe^{2+}-Ti^{4+} intervalence bands are observed in the same region as the feature in the rotherkopfite spectrum. They occur at about 488 nm in andalusite (Smith and Strens, 1976; Taran and Koch-Müller, 2011); at about 440 nm in dravite tourmaline (Smith and Strens, 1976); and in the 400–460 nm region in taramellite, traskite and neptunite (Mattson and Rossman, 1988). This makes Fe^{2+}–Ti^{4+} IVCT a prime candidate for explaining the absorption feature in the rotherkopfite spectrum. The width of the absorption bands also indicates that they come from IVCT. It was previously observed that large half widths are generally the most reliable characteristic of charge transfer transitions (Mattson and Rossman, 1987). IVCT bands generally have much greater widths than absorption bands from single metal ions, which are usually less than 3000 cm^{-1}.

Table 3. Powder X-ray diffraction data (d in Å) for rotherkopfite ($I_{calc} > 2.5$).

I_{obs}	d_{obs}	d_{calc}	I_{calc}	hkl
100	9.63	9.5796	100	1 1 0
33	7.76	7.7522	32	$\bar{1}$ 1 1
6	5.85	5.8187	5	1 1 1
17	4.54	4.5285	15	0 0 2
		3.8499	7	$\bar{1}$ 3 1
		3.7125	3	1 1 2
24	3.537	3.5275	33	1 3 1
38	3.339	3.3164	25	$\bar{3}$ 3 1
48	3.198	3.1932	57	3 3 0
		3.0975	12	$\bar{5}$ 1 2
		3.0408	6	$\bar{3}$ 3 2
67	2.952	2.9537	54	$\bar{2}$ 2 3
		2.9094	22	2 2 2
37	2.867	2.8874	13	5 1 0
		2.8469	33	1 3 2
		2.7777	5	3 3 1
14	2.752	2.7426	17	$\bar{5}$ 1 3
		2.7247	3	3 1 2
21	2.560	2.5641	16	$\bar{1}$ 3 3
27	2.510	2.4971	23	$\bar{6}$ 2 2
33	2.479	2.4808	23	$\bar{6}$ 2 1
		2.4665	13	5 1 1
		2.4145	6	$\bar{4}$ 4 2
15	2.316	2.3184	6	$\bar{5}$ 1 4
		2.3095	11	$\bar{7}$ 1 2
13	2.285	2.2894	6	1 3 3
		2.2822	4	2 2 3
6	2.248	2.2585	6	$\bar{7}$ 1 1
		2.2403	3	$\bar{1}$ 5 2
		2.2178	5	$\bar{7}$ 1 3
35	2.179	2.1751	33	0 4 3
		2.1567	4	3 1 3
27	2.091	2.1080	3	1 5 2
		2.0884	13	$\bar{6}$ 2 4
		2.0773	9	1 1 4
		2.0709	3	5 1 2
19	2.059	2.0568	13	$\bar{8}$ 0 2
		2.0418	7	6 2 1
9	2.018	2.0125	10	2 6 0
12	1.9871	1.9906	3	$\bar{5}$ 5 1
		1.9852	6	$\bar{1}$ 5 3
16	1.9247	1.9250	8	$\bar{2}$ 6 2
		1.9175	8	2 6 1
6	1.8743	1.8784	6	$\bar{1}$ 1 5
		1.8046	3	$\bar{9}$ 1 2
11	1.7677	1.7735	4	$\bar{2}$ 6 3
		1.7638	7	2 6 2
8	1.6895	1.6954	5	1 1 5
		1.6899	3	$\bar{4}$ 4 5
		1.6741	3	$\bar{4}$ 0 6
11	1.6598	1.6633	3	4 4 3
		1.6534	3	$\bar{6}$ 6 1
		1.6496	4	3 5 3
12	1.6139	1.6191	5	7 5 0
		1.6005	3	$\bar{2}$ 6 4
19	1.5862	1.5890	13	$\bar{10}$ 2 3
		1.5820	5	$\bar{10}$ 2 2
		1.5735	5	$\bar{3}$ 7 3
11	1.5580	1.5682	6	0 8 0
		1.5597	5	$\bar{1}$ 1 6
		1.5487	4	$\bar{10}$ 2 4
		1.5295	3	$\bar{10}$ 2 1
34	1.5110	1.5087	35	$\bar{8}$ 4 5
31	1.4802	1.4805	22	8 4 1
		1.4735	3	$\bar{7}$ 5 5
		1.4547	6	4 4 4
9	1.4213	1.4289	3	$\bar{9}$ 5 4
		1.4235	5	2 6 4
		1.4128	3	$\bar{7}$ 7 1
23	1.3898	1.3997	5	$\bar{7}$ 1 7
		1.3928	5	$\bar{6}$ 2 7
		1.3904	4	4 8 1
		1.3879	9	1 9 0
		1.3802	4	$\bar{1}$ 9 1
18	1.3652	1.3624	11	6 2 4
		1.3590	7	$\bar{9}$ 5 5

Table 4. Data collection and structure refinement for rotherkopfite.

Diffractometer	Rigaku R-Axis Rapid II
X-ray radiation	Mo$K\alpha$ ($\lambda = 0.71075$ Å)
Temperature	293(2) K
Structural formula	$(K_{0.746}Na_{0.254})Na_{1.866}(Fe^{2+}_{0.500}Ti_{0.309}Mg_{0.119}\square_{0.084})_2$ $(Ti_{0.410}Fe^{2+}_{0.340}Mg_{0.250})_2(Fe^{2+}_{0.485}Li_{0.144}Ti_{0.078}\square_{0.293})\ Si_{7.45}O_{24}$
Space group	$C2/c$ (#15)
Unit-cell dimensions	$a = 16.4599(17)$ Å $b = 12.5457(6)$ Å $c = 10.0487(7)$ Å $\beta = 115.669(7)°$
V	1870.3(3) Å^3
Z	4
Density (for the above formula)	3.138 g cm^{-3}
Absorption coefficient	3.125 mm^{-1}
$F(000)$	1738.7
Crystal size	60 × 60 × 60 µm
θ range	3.25 to 24.99°
Index ranges	$-19 \le h \le 19$, $-14 \le k \le 14$, $-11 \le l \le 11$
Reflections collected/unique	6861/1630; $R_{int} = 0.043$
Reflections with $I > 2\sigma_I$	1324
Completeness to $\theta = 24.99°$	99.2 %
Refinement method	Full-matrix least squares on F^2
Parameters/constraints	189/0
Goodness of fit	1.064
Final R indices [$I > 2\sigma_I$]	$R_1 = 0.0268$, $wR_2 = 0.0406$
R indices (all data)	$R_1 = 0.0383$, $wR_2 = 0.0441$
Extinction coefficient	0.00029(7)
Largest difference peak/hole	$+0.40/-0.37\ e$/Å^3

$R_{int} = \Sigma|F_o^2 - F_o^2(\text{mean})|/\Sigma[F_o^2]$. Goodness of fit $= S = \{\Sigma[w(F_o^2 - F_c^2)^2]/(n-p)\}^{1/2}$. $R_1 = \Sigma||F_o| - |F_c||/\Sigma|F_o|$.
$wR_2 = \{\Sigma[w(F_o^2 - F_c^2)^2]/\Sigma[w(F_o^2)^2]\}^{1/2}$; $w = 1/[\sigma^2(F_o^2) + (aP)^2 + bP]$, where a is 0.0025, b is 4.85 and P is $[2F_c^2 + \text{Max}(F_o^2, 0)]/3$.

7 Crystallography

7.1 X-ray powder diffraction

X-ray powder diffraction data were recorded using a Rigaku R-Axis Rapid II curved imaging plate microdiffractometer with monochromatized Mo$K\alpha$ radiation. A Gandolfi-like motion on the ϕ and ω axes was used to randomize the sample. Observed d values and intensities were derived by profile fitting using the JADE Pro software (Materials Data, Inc.). Data are given in Table 3. Refined monoclinic unit-cell parameters (space group $C2/c$) are $a = 16.52(3)$, $b = 12.56(3)$, $c = 10.05(3)$ Å, $\beta = 115.82(6)°$ and $V = 1877(8)$ Å^3.

7.2 Single-crystal diffraction

Single-crystal X-ray studies were also done using a Rigaku R-Axis Rapid II curved imaging plate microdiffractometer with monochromatized Mo$K\alpha$ radiation. The Rigaku CrystalClear software package was used for processing the structure data, including the application of an empirical absorption correction using the multi-scan method with ABSCOR (Higashi, 2001). The structure was solved using the intrinsic-phasing algorithm of SHELXT (Sheldrick, 2015a). SHELXL-2016 (Sheldrick, 2015b) was used for the refinement of the structure. The structure solution in space group $I2/a$ located all cation and O sites. The structure solution showed the mineral to be isostructural with neptunite-group minerals. Consequently, the cell and atom coordinated were transformed to be consistent with those reported for magnesioneptunite (Karimova et al., 2012) in space group $C2/c$. Attempts to refine the structure in Cc provided poorer results, including higher R factors and numerous sites with nonpositive definite anisotropic displacement parameters.

With all O sites assigned full occupancy, an initial refinement indicated all four Si sites to have slightly less than full occupancy (consistent with the EPMA formulas). Attempts to refine the occupancies of all cation sites at the same time resulted in unstable refinements; therefore, each of the Si sites was at this stage assigned an occupancy of 0.95. The Na site was assigned full occupancy. The K site was refined with join occupancy by K and Na. Three octahedrally coordinated cation sites ($M1$, $M2$ and $M3$) were refined with joint

occupancies by Fe and Mg to assess their site-scattering values. $M1$ refined to $Fe_{0.654(4)}Mg_{0.346(4)}$ for a site-scattering value of 169.25. $M2$ refined to $Fe_{0.628(4)}Mg_{0.372(4)}$ for a site-scattering value of 166.34. $M3$ refined to $Mg_{0.806(5)}Fe_{0.194(5)}$ for a site-scattering value of 58.86.

For assigning the cations to the $M1$, $M2$ and $M3$ sites, the program OccQP (Wright et al., 2000) was used. This program uses quadratic equations in a constrained least-squares formulation to optimize occupancy assignments based upon site scattering, chemical composition, charge balance, bond valence and cation–anion bond lengths. In the OccQP analysis, the chemical composition (based on the empirical formula), bond valence and site scattering were all allowed to vary with equal weighting. OccQP initially assigned Li to the $M1$ site; however, bond distances indicate that it is much more likely to be hosted at the $M3$ site, so it was constrained to that site. The resulting site occupancies are $M1 = Fe^{2+}_{0.500}Ti_{0.309}Mg_{0.119}\square_{0.084}$ (site-scattering value = 169.76), $M2 = Ti_{0.410}Fe^{2+}_{0.340}Mg_{0.250}$ (site-scattering value = 166.86) and $M3 = Fe^{2+}_{0.485}Li_{0.144}Ti_{0.078}\square_{0.293}$ (site-scattering value = 58.98).

In the final refinement, the OccQP-calculated occupancies were assigned to the M sites. The K site occupancy refined to $K_{0.746(11)}Na_{0.254(11)}$, the Na site occupancy refined to 0.933(5), and the Si1, Si2, Si3 and Si4 site occupancies refined to 0.930(4), 0.933(4), 0.925(4) and 0.938(4), respectively. The O sites all refined well at full occupancies. The structural formula based upon these site assignments is $(K_{0.746}Na_{0.254})Na_{1.866}{}^{M1}(Fe^{2+}_{0.500}Ti_{0.309}Mg_{0.119}\square_{0.084})_2{}^{M2}(Ti_{0.410}Fe^{2+}_{0.340}Mg_{0.250})_2{}^{M3}(Fe^{2+}_{0.485}Li_{0.144}Ti_{0.078}\square_{0.293})\ Si_{7.45}O_{24}$ or, grouped in the same way as the empirical formula, $(K_{0.746}Na_{0.254})_{\Sigma 1.00}(Na_{1.866}\square_{0.134})_{\Sigma 2.00}(Fe^{2+}_{1.680}Ti_{1.438}Mg_{0.738}\square_{0.144})_{\Sigma 4.00}(Fe^{2+}_{0.485}Li_{0.144}Ti_{0.078}\square_{0.293})_{\Sigma 1.00}(Si_{7.450}\square_{0.550})_{\Sigma 8.00}O_{24}$. The latter formula is in reasonable agreement with the empirical formula noted above.

The data collection and refinement details are given in Table 4, atom coordinates and displacement parameters in Table 5, selected bond distances in Table 6, and a bond-valence analysis in Table 7.

8 Discussion

Rotherkopfite is isostructural with members of the neptunite group (Table 1). The structure (Fig. 5) is based on two interwoven three-dimensional frameworks: (1) a silicate framework made up of pyroxene-like chains of corner-sharing SiO_4 tetrahedra running along the [110] and $[\bar{1}10]$ directions, which are linked to one another in the [001] direction by sharing corners, and (2) an octahedral framework made up of chains of edge-sharing metal–oxygen octahedra, centred by $M1$ and $M2$ cations, also running along the [110] and $[\bar{1}10]$ directions, which are linked to one another in the [001] direction by edge sharing with $M3$-centred octahedra. The two

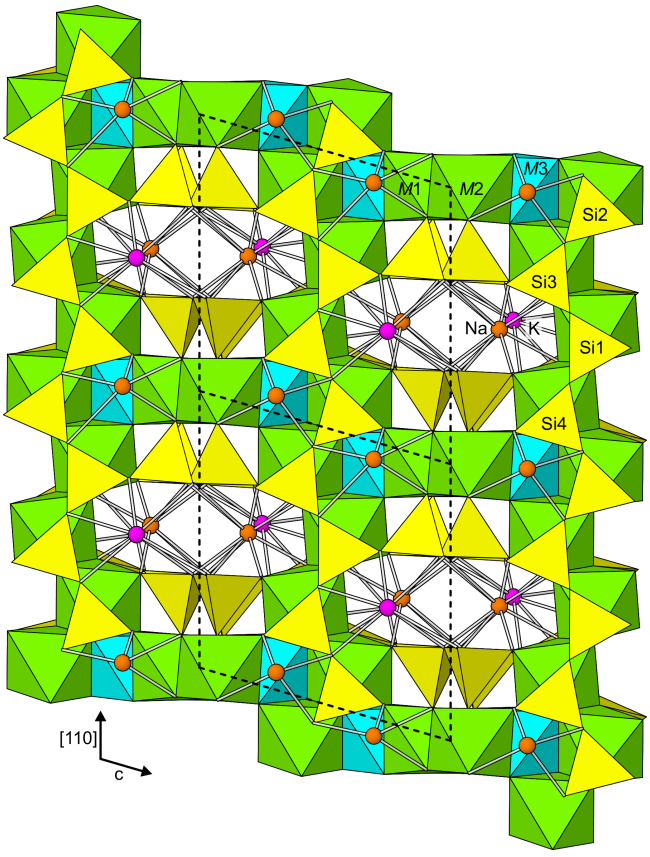

Figure 5. The structure of rotherkopfite viewed along $[1\bar{1}0]$. The unit-cell outline is shown by dashed lines.

interwoven frameworks are bound to one another by corner sharing. K and Na are hosted in channels in the combined framework.

Rotherkopfite differs from all of the other neptunite-group minerals in that the $M3$ site (labelled Li in the other structures) is dominated by Fe^{2+} rather than Li. Interestingly, the O9 site, which is the only non-silicate O site, has a very low bond-valence sum (BVS) of 1.21 vu. This suggests that, unlike for other members of the neptunite group, this site may be an OH group. However, as noted above, spectroscopic evidence indicates that rotherkopfite is anhydrous. It is worth noting that the O9 site in the structure of magnesioneptunite (Karimova et al., 2012) has a rather low BVS of 1.50 vu. The low BVS value for O9 in rotherkopfite may be related to the apparently "stressed" nature of the site as suggested by the elongated displacement ellipsoids of the O9, $M1$ and $M2$ sites along the direction of the bond O4–$M2$–O9–$M1$–O7. It is evident that O9 exhibits a static disorder that can be related to Fe^{2+}–O–Ti and Ti–O–Fe^{2+} alternating configurations.

Table 5. Refined atom coordinates, displacement parameters (Å^2) and site occupancies for rotherkopfite.

	x/a	y/b	z/c	U_{eq}	Occupancy
K	0.5	0.08555(11)	0.25	0.0286(5)	$K_{0.746(11)}Na_{0.254(11)}$
Na	0.26277(8)	0.19917(11)	0.80550(15)	0.0216(5)	0.933(5)
*M*1	0.08825(3)	0.06017(5)	0.61211(6)	0.01216(17)	$Fe^{2+}_{0.500}Ti_{0.309}Mg_{0.119}\square_{0.084}$
*M*2	0.16153(3)	0.18078(5)	0.40409(6)	0.01192(17)	$Ti_{0.410}Fe^{2+}_{0.340}Mg_{0.250}$
*M*3	0	−0.06299(9)	0.75	0.0121(3)	$Fe^{2+}_{0.485}Li_{0.144}Ti_{0.078}\square_{0.293}$
Si1	0.35576(5)	0.09298(7)	0.44136(9)	0.0065(3)	0.930(4)
Si2	0.10681(5)	0.14909(7)	0.92017(9)	0.0072(3)	0.933(4)
Si3	0.27129(5)	0.02428(7)	0.11131(10)	0.0064(3)	0.925(4)
Si4	0.52457(5)	0.22698(7)	0.58657(9)	0.0074(3)	0.938(4)
O1	0.34129(13)	0.04864(17)	0.2804(2)	0.0165(5)	1
O2	0.46314(12)	0.11900(16)	0.5267(2)	0.0150(5)	1
O3	0.10982(13)	0.16884(17)	0.7661(2)	0.0169(5)	1
O4	0.29174(13)	0.19288(17)	0.4284(2)	0.0164(5)	1
O5	0.20822(12)	0.07759(16)	0.5934(2)	0.0156(5)	1
O6	0.21240(12)	0.13255(16)	0.0462(2)	0.0152(5)	1
O7	0.04328(12)	0.17402(17)	0.4305(2)	0.0172(5)	1
O8	0.33461(13)	−0.00742(16)	0.5252(2)	0.0152(5)	1
O9	0.13041(13)	−0.06097(18)	0.7645(3)	0.0233(6)	1
O10	0.07277(13)	0.25657(16)	0.9738(2)	0.0158(5)	1
O11	0.10488(13)	0.28782(17)	0.2475(2)	0.0170(5)	1
O12	0.04740(12)	0.04762(17)	0.9299(2)	0.0151(5)	1

	U^{11}	U^{22}	U^{33}	U^{23}	U^{13}	U^{12}
K	0.0149(7)	0.0507(10)	0.0192(8)	0	0.0066(5)	0
Na	0.0168(8)	0.0262(10)	0.0232(9)	−0.0088(7)	0.0099(6)	−0.0060(6)
M1	0.0082(3)	0.0166(3)	0.0106(3)	−0.0053(3)	0.0031(2)	−0.0002(2)
M2	0.0103(3)	0.0157(3)	0.0114(3)	0.0066(3)	0.0062(2)	0.0047(2)
M3	0.0114(5)	0.0137(6)	0.0106(6)	0	0.0043(4)	0
Si1	0.0066(5)	0.0069(5)	0.0062(5)	−0.0009(4)	0.0029(4)	−0.0001(3)
Si2	0.0073(5)	0.0074(5)	0.0067(5)	−0.0003(4)	0.0029(4)	−0.0001(3)
Si3	0.0051(5)	0.0081(5)	0.0053(5)	−0.0007(4)	0.0017(4)	−0.0001(3)
Si4	0.0079(5)	0.0070(5)	0.0073(5)	−0.0007(4)	0.0033(4)	−0.0007(3)
O1	0.0164(11)	0.0184(12)	0.0129(12)	−0.0014(10)	0.0045(9)	0.0011(9)
O2	0.0145(11)	0.0141(12)	0.0150(12)	−0.0026(10)	0.0050(9)	−0.0020(9)
O3	0.0172(11)	0.0195(12)	0.0139(12)	−0.0012(10)	0.0065(9)	−0.0024(10)
O4	0.0168(11)	0.0169(13)	0.0164(12)	0.0016(10)	0.0081(9)	0.0028(9)
O5	0.0135(11)	0.0140(12)	0.0177(12)	0.0000(10)	0.0052(9)	0.0016(9)
O6	0.0131(11)	0.0129(12)	0.0169(12)	−0.0004(10)	0.0041(9)	−0.0009(9)
O7	0.0172(11)	0.0142(12)	0.0231(13)	−0.0004(10)	0.0116(10)	0.0014(9)
O8	0.0149(11)	0.0150(12)	0.0176(12)	0.0027(10)	0.0089(9)	0.0014(9)
O9	0.0174(11)	0.0241(14)	0.0305(14)	−0.0138(12)	0.0123(10)	−0.0038(10)
O10	0.0170(11)	0.0136(12)	0.0185(13)	0.0009(10)	0.0092(9)	0.0002(9)
O11	0.0154(11)	0.0188(13)	0.0150(12)	0.0009(10)	0.0048(9)	0.0002(9)
O12	0.0166(11)	0.0136(12)	0.0169(12)	0.0004(10)	0.0090(9)	−0.0006(9)

Table 6. Selected bond distances [Å] for rotherkopfite.

K–O1 (× 2)	2.797(2)	*M*1–O3	1.976(2)	Si1–O4	1.606(2)
K–O10 (× 2)	2.843(2)	*M*1–O9	2.053(2)	Si1–O1	1.627(2)
K–O8 (× 2)	2.854(2)	*M*1–O5	2.075(2)	Si1–O2	1.629(2)
K–O2 (× 2)	3.121(2)	*M*1–O12	2.0907(19)	Si1–O8	1.634(2)
K–O2 (× 2)	3.288(2)	*M*1–O12	2.137(2)	⟨Si1–O⟩	1.624
⟨K–O⟩	2.981	*M*1–O7	2.179(2)		
		⟨*M*1–O⟩	2.085	Si2–O3	1.590(2)
Na–O3	2.403(2)			Si2–O12	1.634(2)
Na–O5	2.453(2)	*M*2–O9	1.966(3)	Si2–O10	1.638(2)
Na–O11	2.462(2)	*M*2–O11	1.969(2)	Si2–O6	1.661(2)
Na–O6	2.514(2)	*M*2–O4	2.055(2)	⟨Si2–O⟩	1.631
Na–O4	2.517(3)	*M*2–O7	2.077(2)		
Na–O10	2.712(2)	*M*2–O5	2.149(2)	Si3–O5	1.607(2)
Na–O6	2.995(3)	*M*2–O4	2.195(2)	Si3–O1	1.616(2)
Na–O8	3.130(3)	⟨*M*2–O⟩	2.069	Si3–O8	1.631(2)
⟨Na–O⟩	2.648			Si3–O6	1.632(2)
		*M*3–O9 (× 2)	2.088(2)	⟨Si3–O⟩	1.622
		*M*3–O12 (× 2)	2.140(2)		
		*M*3–O7 (× 2)	2.149(2)	Si4–O11	1.595(2)
		⟨*M*3–O⟩	2.126	Si4–O7	1.629(2)
				Si4–O2	1.641(2)
				Si4–O10	1.654(2)
				⟨Si4–O⟩	1.630

Table 7. Bond-valence analysis for rotherkopfite. Values are expressed in valence units (vu).

	K	Na	*M*1	*M*2	*M*3	Si1	Si2	Si3	Si4	sum
O1	$0.13_{\times 2\downarrow}$					0.92		0.94		1.99
O2	$0.06_{\times 2\downarrow}$					0.92			0.90	1.92
	$0.04_{\times 2\downarrow}$									
O3		0.17	0.49				1.02			1.68
O4		0.13		0.44		0.97				1.85
				0.31						
O5		0.15	0.38	0.34				0.97		1.84
O6		0.13					0.85	0.91		1.93
		0.04								
O7			0.30	0.41	$0.22_{\times 2\downarrow}$				0.93	1.86
O8	$0.11_{\times 2\downarrow}$	0.03				0.91		0.91		1.96
O9			0.41	0.55	$0.25_{\times 2\downarrow}$					1.21
O10	$0.12_{\times 2\downarrow}$	0.08					0.90		0.87	1.97
O11		0.15		0.54					1.01	1.70
O12			0.37		$0.22_{\times 2\downarrow}$		0.91			1.83
			0.33							
sum	0.92	0.88	2.28	2.59	1.38	3.72	3.68	3.73	3.71	

Bond-valence parameters are from Gagné and Hawthorne (2015). Note that bond-valence values are based on the occupancies of the cation sites.

Data availability. Crystallographic data for rotherkopfite are available in the Supplement.

Supplement. The supplement related to this article is available online at: https://doi.org/10.5194/ejm-36-605-2024-supplement.

Author contributions. ARK oversaw the research, determined the physical and optical properties, did the X-ray diffraction studies, and wrote the paper. GM and JD conducted the initial characterization studies on the specimen and identified it as a potentially new species. CM did the electron microprobe analyses. GRR conducted the FTIR and optical absorption spectroscopic studies. YG did the lithium analyses.

Competing interests. The contact author has declared that none of the authors has any competing interests.

Disclaimer. Publisher's note: Copernicus Publications remains neutral with regard to jurisdictional claims made in the text, published maps, institutional affiliations, or any other geographical representation in this paper. While Copernicus Publications makes every effort to include appropriate place names, the final responsibility lies with the authors.

Special issue statement. This article is part of the special issue "New minerals: EJM support". It is not associated with a conference.

Acknowledgements. Andrei Zolotarev and an anonymous reviewer are thanked for their constructive comments on the manuscript.

Financial support. A portion of this study was funded by the John Jago Trelawney Endowment to the Mineral Sciences Department of the Natural History Museum of Los Angeles County.

Review statement. This paper was edited by Sergey Krivovichev and reviewed by Andrei Zolotarev and one anonymous referee.

References

Bell, D. R., Rossman, G. R., Maldener, J., Endisch, D., and Rauch, F.: Hydroxide in olivine: A quantitative determination of the absolute amount and calibration of the IR spectrum, J. Geophys. Res., 108, 2105, https://doi.org/10.1029/2001JB000679, 2003.

Chukanov, N. V., Rastsvetaeva, R. K., Aksenov, S. M., Pekov, I. V., Zubkova, N. V., Britvin, S. N., Belakovskiy, D. I., Schueller, W., and Ternes, B.: Günterblassite, $(K,Ca)_{3-x}Fe[(Si,Al)_{13}O_{25}(OH,O)_4]\cdot 7H_2O$, a new mineral: the first phyllosilicate with triple tetrahedral layer, Geol. Ore Dep., 54, 656–662, 2012.

Chukanov, N. V., Rastsvetaeva, R. K., Aksenov, D. M., Blass, G., Pekov, I. V., Belakovskiy, D. I., Tschörtner, J., Schüller, W., and Ternes, B.: Emmerichite, $Ba_2Na(Na,Fe^{2+})_2(Fe^{3+},Mg)Ti_2(Si_2O_7)_2O_2F_2$, a new lamprophyllite-group mineral from the Eifel volcanic region, Germany, New Data Min., 49, 5–13, 2014.

Gagné, O. C. and Hawthorne, F. C.: Comprehensive derivation of bond-valence parameters for ion pairs involving oxygen, Acta Crystallogr. B, 71, 562–578, 2015.

Gunter, M. E., Bandli, B. R., Bloss, F. D., Evans, S. H., Su, S. C., and Weaver, R.: Results from a McCrone spindle stage short course, a new version of EXCALIBR, and how to build a spindle stage, Microscope, 52, 23–39, 2004.

Higashi, T.: ABSCOR, Rigaku Corporation, Tokyo, 2001.

Karimova, O. V., Yakubovich, O. V., Zadov, A. E., Ivanova, A. G., and Urusov, V. S.: Crystal structure of magnesioneptunite, Crystallogr. Rep., 57, 505–513, 2012.

Kunz, M., Armbruster, T., Lager, G. A., Schultz, A. J., Goyette, R. J., Lottermoser, W., and Amthauer, G.: Fe, Ti ordering and octahedral distortions in acentric neptunite: Temperature dependent X-ray and neutron structure refinements and Mössbauer spectroscopy, Phys. Chem. Miner., 18, 199–213, 1991.

Mandarino, J. A.: The Gladstone-Dale relationship: Part IV. The compatibility concept and its application, Can. Mineral., 19, 441–450, 1981.

Matsubara, S., Miyawaki, R., Kurosawa, M., and Suzuki, Y.: Watatsumiite, $KNa_2LiMn_2V_2Si_8O_{24}$, a new mineral from the Tanohata mine, Iwate Prefecture, Japan, J. Miner. Petrol. Sci., 98, 142–150, 2003.

Mattson, S. M. and Rossman G. R.: Identifying characteristics of charge transfer transitions in minerals, Phys. Chem. Miner., 14, 94–99, 1987.

Mattson, S. M. and Rossman G. R.: Fe^{2+}-Ti^{4+} charge transfer in stoichiometric Fe^{2+},Ti^{4+}-minerals, Phys. Chem. Miner., 16, 78–82, 1988.

Rossman, G. R. and Taran, M. N.: Spectroscopic standards for four- and five-coordinated Fe^{2+} in oxygen-based minerals, Am. Mineral., 86, 896–903, 2001.

Sheldrick, G. M.: SHELXT – Integrated space-group and crystal-structure determination, Acta Crystallogr. A, 71, 3–8, 2015a.

Sheldrick, G. M.: Crystal Structure refinement with SHELX, Acta Crystallogr. C, 71, 3–8, 2015b.

Smith, G. and Strens, R. G. H.: Intervalence transfer absorption in some silicate, oxide and phosphate minerals, in: The Physics and Chemistry of Minerals and Rocks, edited by: Strens, R. G. J., New York, Wiley and Sons, 583–612, 1976.

Taran, M. N. and Koch-Müller, M.: Optical absorption of electronic Fe–Ti charge-transfer transition in natural andalusite: the thermal stability of the charge-transfer band, Phys. Chem. Miner., 38, 215–222, 2011.

Wright, S. E., Foley, J. A., and Hughes, J. M.: Optimization of site occupancies in minerals using quadratic programming, Am. Mineral., 85, 524–531, 2000.

Zolotarev, A. A., Krivovichev, S. V., and Yakovenchuk, V. N.: Refinement of the mangan-neptunite crystal structure, Geol. Ore Dep., 49, 835–838, 2007.